ACS Photonics

pubs.acs.org/journal/apchd5
Article

Air-Stable Room-Temperature Quasi-2D Tin Iodide Perovskite Microlasers

Sangyeon Cho,[¶] Wenhao Shao,[¶] Jeong Hui Kim, Letian Dou,* and Seok-Hyun Yun*

Cite This: ACS Photonics 2026, 13, 2367−2374
Read Online

ACCESS | Metrics & More | Article Recommendations | Supporting Information

ABSTRACT: Quasi-2D tin iodide perovskites (TIPs) are promising lead-free alternatives for optoelectronic applications, but achieving stable lasing remains challenging due to their limited environmental stability. Here, we report air-stable, room-temperature lasing from quasi-2D TIP microcrystals as small as 4 μm. Incorporation of the organic spacer 5IPA3 significantly enhanced the stability of these materials compared with previously reported TIPs. Lasing was observed from both dielectric (n = 4) and plasmonic (n = 3 and n = 4) TIP microlasers. Under picosecond pumping, lasing was sustained for over 10^8 pump pulses in ambient conditions. These results represent a significant step toward practical photonic applications of tin-based perovskites.

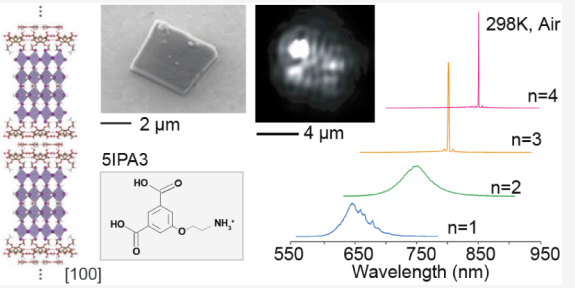

KEYWORDS: *tin iodide perovskite, quasi-2D, microlaser, plasmonics, environmental stability*

INTRODUCTION

Lead halide perovskites (LHPs) have attracted significant attention due to their exceptional performance in a range of optoelectronic technologies, including photovoltaics,[1] light-emitting diodes,[2] and lasers.[3] However, concerns about lead toxicity[4] and environmental risks[5] have spurred interest in alternative compositions. Among these, tin iodide perovskites (TIPs) have been proposed[6] and are currently under active investigation as leading lead-free candidates for optoelectronic applications.[7] TIPs offer even higher carrier mobility[8] and lower nonradiative losses[9] than their lead counterparts. TIP-based solar cells have achieved power conversion efficiencies exceeding 14%[10] and operational stability beyond 1,300 h in nitrogen-purged environments.[11] Moreover, animal toxicity assays have shown no clear evidence of acute toxicity or genetic-level risks associated with TIPs.[12] Despite these advantages, their primary limitations remain the poor material stability and fabrication reproducibility, largely due to the high susceptibility of Sn(II) to oxidation into Sn(IV)[13] and poor thermal instabilities.[14] Oxidation susceptibility and low defect formation energy facilitate vacancy formation and accelerate degradation in the presence of air, moisture, and light.[15,16]

Recently, Ruddlesden−Popper perovskites, which consist of two-dimensional (2D) or quasi-2D perovskite slabs separated by cationic spacers, have attracted growing interest.[17,18] The quantum-well architecture imparts distinctive physical and optical characteristics, influencing charge transport,[19,20] exciton dynamics,[18,21] and ferroelasticity.[22−24] The spacer layers not only provide structural versatility but also help suppress oxygen permeation and improve photostability compared to 3D bulk counterparts.[19,20] Ruddlesden−Popper TIPs, incorporating various spacers and layer thicknesses, have been actively explored for lasing and related applications. Optically pumped lasing has been demonstrated from PEA-incorporated 2D TIPs using a high-Q distributed feedback resonator at 77 K.[25] Lasing from TIP microflakes incorporating diverse cations such as PEA (phenylethylammonium), 2T+ (bithiophenylethylammonium), and 3T+ (2-([2,2″:5′,2″-terthiophen]-5-yl)ethan-1-aminium) has exhibited lasing at 83 K in nitrogen.[26] Similarly, lasing has been observed at 88 K in argon from ∼100 μm-long TIP nanowires synthesized using BrCA3 (2-(2-bromo-5-carboxyphenoxy)ethan-1-aminium).[27] However, achieving stable lasing under ambient conditions has remained an unresolved challenge for TIPs.

In this study, we demonstrate room-temperature lasing in air from quasi-2D TIPs incorporating 2-(3,5-dicarboxyphenoxy)-ethan-1-aminium (5IPA3) as the organic spacer. The 5IPA3 molecule, bearing two carboxyl groups, forms robust and highly directional hydrogen bonds with the perovskite slabs. This hydrogen-bonding network not only reduces oxygen permeability but also increases the mechanical rigidity of the lattice,[28] which is believed to enhance thermal stability under high optical pumping conditions.[25,29] The resulting material, $(5IPA3)_2(MA)_{n-1}Sn_nI_{3n+1}$ (where MA is methylammonium, n represents the number of perovskite layers between organic

Received: September 22, 2025
Revised: December 31, 2025
Accepted: January 6, 2026
Published: February 24, 2026

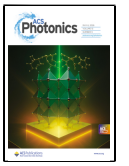

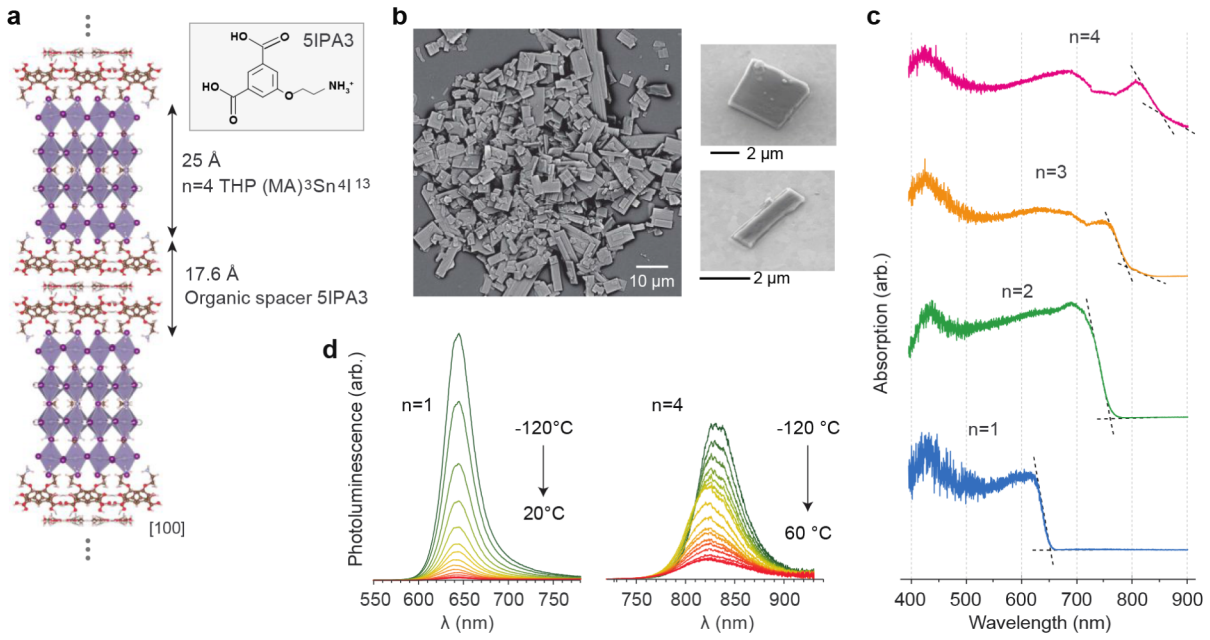

Figure 1. Material properties of layered tin iodide perovskite with a 5IPA3 spacer. (a) Crystal structure of 5IPA3-n4 projected along [010]. The alternating organic and inorganic lattices have thicknesses of 17.6 and 24.0 Å, respectively. (b) A representative scanning electron microscopy (SEM) image of abundant microcrystals produced by sonication. (c) Diffuse reflectance spectra of $(5IPA3)_2(MA)_{n-1}Sn_nI_{3n+1}$ microcrystals with n = 1 to 4. Dashed lines: linear fits to the absorption edge. (d) Temperature-dependent photoluminescence spectroscopy of 5IPA3-n4 and 5IPA3-n1 microcrystals.

spacers), exhibited substantially improved ambient stability both in the dark and under photoexcitation compared to well-known 2D PEA-TIPs. Notably, we achieved, for the first time to our knowledge, air-stable room-temperature lasing from quasi-2D TIP microcrystals (n = 3 and 4) under ambient conditions. This achievement represents a milestone in the development of lead-free perovskites and advances their potential for photonic and optoelectronic applications.

2D TIN IODIDE PEROVSKITES WITH 5IPA3 SPACER

Benzoic acid was chosen as the molecular backbone of 5IPA3, as inspired by the recently developed molecular templating methods[27] to permutate the anisotropy in organic sublattices using robust and directional H-bonded networks. Specifically, the benzene-1,3-dicarboxylic acid core was introduced to create a sophisticated organic network to reduce the permeability of air and moisture. Details of the spacer design and crystal growth methods are described elsewhere. Phase-pure quasi-2D perovskites exhibited trends where higher n values yield higher optical gain.[26,30] Figure 1a depicts the crystal structure of $(5IPA3)_2(MA)_3Sn_4I_{13}$ for n = 4. The thickness of the organic sublattice is ∼17.6 Å, and that of the inorganic perovskite layer is ∼24 Å. The dielectric permittivity of 5IPA3-n4 is approximately 4.[31] Considering the subnanometer-thick organic lattices, it is expected to allow subpicosecond out-of-plane exciton transport via tunneling[32] and out-of-plane exciton diffusion lengths of ∼100 nm.[33] 5IPA3-n4 microcrystals were obtained by breaking down bulk crystals via sonication (Figure 1b).[27] The resulting microplates had a median length of 13 μm and a mean width of 2 μm (Figures S1 and S2). The median thickness of the microplates was 545 nm, which corresponds to a total of 131 quantum wells.

Figure 1c presents the diffuse reflectance spectra of microcrystals with different n values from 1 to 4. The quantum-well band edge energy was estimated from the onset of the absorption edges, which are 1.44 eV for 5IPA3-n4 (n = 4), 1.54 eV for 5IPA3-n3 (n = 3), 1.63 eV for 5IPA3-n2 (n = 2), and 1.91 eV for 5IPA3-n1 (n = 1). Stronger exciton binding in lower n phases increases both the higher Auger recombination rate[34] and exciton−phonon coupling.[35] Additionally, in the electron−hole plasma lasing scenario,[36−38] the smaller exciton Bohr radius at lower n leads to a higher carrier density for transparency.[39] Figure 1d shows photoluminescence (PL) spectra from microcrystals for n = 1 and 4, excited by 375 nm light, at different ambient temperatures from −120 to 60 °C. By fitting the PL intensity dependence on temperature using $I(T) \propto 1/(1 + A\, e^{-E_b/k_BT})$, we estimated exciton binding energy E_b. E_b is the highest for 5IPA3-n1, reaching a value of 132 ± 3 meV. E_b decreases with increasing n, reaching a value of 94 ± 8 meV for 5IPA3-n4 (Figure S3). By fitting the emission spectra near the band edge, we derived electronic temperature (T_e) and estimated Mott transition density for transparency. Considering the thickness of the organic spacer layer and an exciton Bohr radius of 0.6 nm adapted from BA_2PbI_4,[41] the 3D Mott transition density for transparency exceeds 10^{19} cm^{-3} (Note S1 and Figure S4). Although this estimation uses parameters adapted from analogous quasi-2D systems, the high value is consistent with the general trend in quantum-well semiconductors—where strong dielectric and quantum confinement reduce the exciton Bohr radius and increase the critical density for exciton−plasma transition.[39] It is noteworthy that excitonic features are less distinct in ensemble absorption spectra due to inhomogeneous broadening or exciton dissociation associated with microplate morphology.

https://doi.org/10.1021/acsphotonics.5c02285
ACS Photonics 2026, 13, 2367−2374

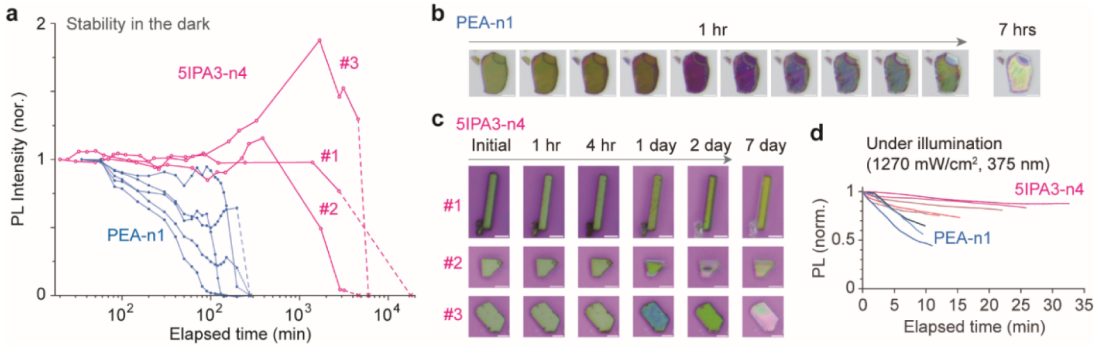

Figure 2. Stability of 5IPA3 TIPs under ambient conditions. (a) PL intensity variation of 5IPA3-n4 microcrystals (pink) and PEA-n1 TIPs (blue). Optical measurements were conducted by using a CW laser at 385 nm with an intensity of 2.77 W/cm^2. (b) Photos of a representative PEA-n1 microcrystal over time stored in the dark condition. (c) Photos of the three 5IPA3-n4 samples in (a) over time. Scale bars: 5 μm. (d) Photostability of 5IPA3-n4 (pink) and PEA-n1 (blue) microcrystals under continuous illumination of 375 nm light at an intensity of 1270 mW/cm^2 in ambient conditions.

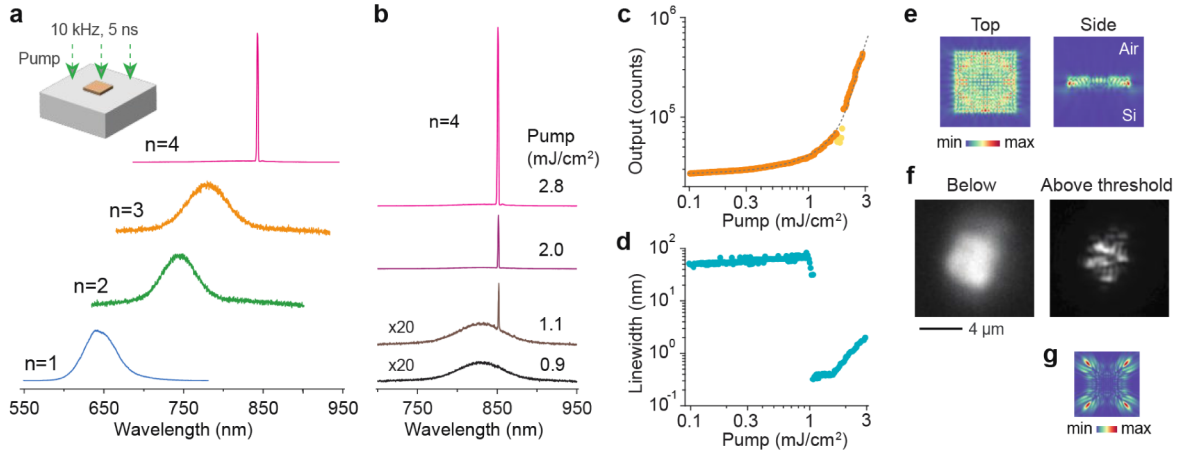

Figure 3. Lasing of 5IPA3-TIP microcrystals in ambient conditions. (a) (top left) Schematic of optically pumped 2D perovskite dielectric laser devices. (bottom) Emission spectra of microcrystals from n = 1 to n = 4 were recorded up to 3 mJ/cm^2. Only 5IPA3-n4 demonstrated lasing. (b) Output spectra at pump fluences of 0.90, 1.11, 2.04, and 2.84 mJ/cm^2. (c) Measured light-in-light-out curve. Dashed line: theoretical fit. (d) Measured line width at different pump fluences. (e) FDTD-simulated electric field amplitude, $|E|$, of the lasing. (f) Measured far-field emission profiles below and above lasing threshold. (g) FDTD simulation for the far-field profile of the lasing mode.

MATERIAL STABILITY AT ROOM TEMPERATURE IN AIR

In bulk $ASnI_3$ perovskites, where "A" represents small organic cations such as MA or formamidinium (FA), Sn(II) to Sn(IV) oxidation produces SnO_2, SnI_4, and AI.[41] SnI_4 and AI are then readily sublimed. A similar degradation route was verified in n = 1 PEA_2SnI_4,[42] as well as other quasi-2D systems. The growth and quality control of microcrystals have dramatic effects on their stability.[43] We measured a half-life of 200 min for bulk $MASnI_3$ films in air using absorbance spectroscopy (Figure S5).

To assess the in-air stability of 5IPA3-n4 TIPs, we tracked the morphology and PL intensity evolution of both 5IPA3-n4 and PEA_2SnI_4 microcrystals (denoted as PEA-n1). The samples were stored in a dark condition between the brief optical measurements. While PEA-n1 microcrystals showed rapid degradation, 5IPA3-n4 maintained stable PL for up to ~1000 min at room temperature in air (Figure 2a). Some 5IPA3-n4 samples (no. 2 and no. 3 in Figure 2a) exhibited a modest increase in PL intensity before it decays and was eventually lost. This is attributed to oxygen-induced defect healing, which is commonly observed in LHPs.[44]

Over time, the original brown/yellow crystals gradually became transparent upon air exposure (Figures 2b and S6). This indicates complete Sn(II) oxidation, as residual MAI and/or SnO_2 have minimal absorption of visible light. Oxidation proceeded from the edges and surfaces toward the center. A dark purple intermediate phase appeared during morphological evolution and disappeared upon full oxidation, often accompanied by a sudden PL drop. This dark phase might correspond to SnI_4 formation within the crystal interior before sublimation, potentially alongside I^- oxidation to I_2, as suggested previously.[45] The dark phase emerged in just 20 min for PEA-n1 (Figure 2b) but was significantly delayed for 5IPA3-n4 to 1−2 days (Figure 2c).

Photostability was evaluated using continuous wave (CW) illumination at 375 nm with 1.3 W/cm^2. Figure 2d presents the PL time series of five individual microcrystals of 5IPA3-n4 and three individual microcrystals of PEA-n1. The mean lifetimes of the exponential PL decay were measured to be approximately 140 min for 5IPA3-n4 and 16 min for PEA-n1 (Table S2). One 5IPA3-n4 sample showed a T90 (90% of initial intensity) of 18.3 min and a half-time (T50) of 3.5 h.

https://doi.org/10.1021/acsphotonics.5c02285
ACS Photonics 2026, 13, 2367−2374

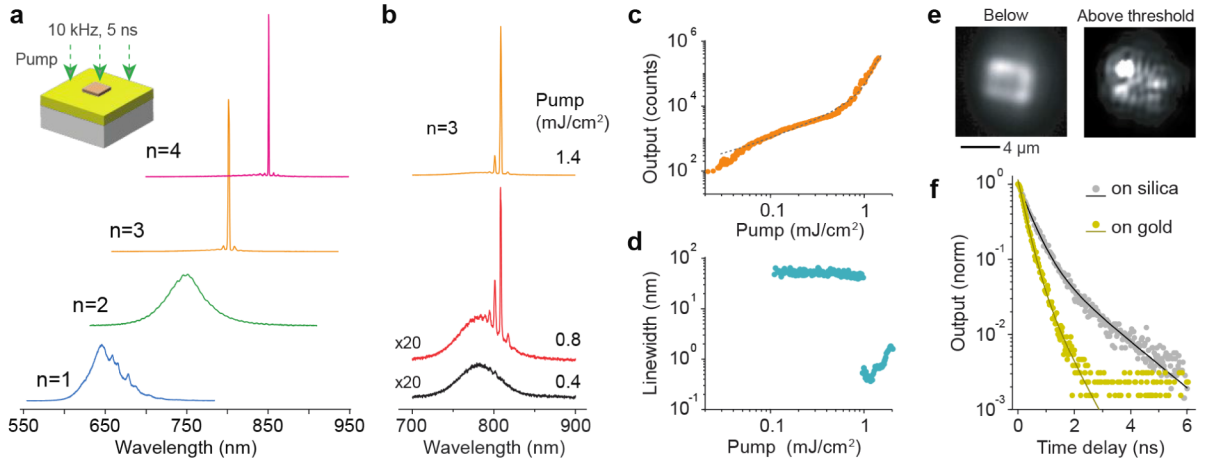

Figure 4. Plasmonic lasing in 5IPA3-TIPs in ambient conditions. (a) (top left) Schematic of an optically pumped 2D perovskite sample on a gold substrate. (bottom) Typical emission spectra from microcrystals with n = 1 to n = 4 phases, at pump fluences of ∼3 mJ/cm^2. 5IPA3-n3 and -n4 samples demonstrated lasing. (b) Output spectra from a 5IPA3-n3 microcrystal at pump fluences of 0.42, 0.81, 1.1, and 1.4 mJ/cm^2. (c) Measured light-in-light-out curve. Dashed line: theoretical fit. (d) Measured line width at different pump fluences. (e) Measured far-field emission profiles below and above the lasing threshold. (f) Transient lifetime decay curves below the threshold from 5IPA3-n4 TIP microcrystals on gold (yellow) and thermal oxide silicon (gray) substrates.

LASING IN AIR AT ROOM TEMPERATURE

We used a custom-built microscope to characterize the lasing properties of microcrystals on a silicon substrate with a 200 nm thick oxide layer. The pump source was a frequency-doubled Q-switched Nd:YAG laser with a pulse width of 5 ns and an emission wavelength of 532 nm. The pump beam size was 30 μm to cover the entire area of the microcrystals. Emission was collected using an objective lens with a numerical aperture of 0.6, and the collected emission spectra were analyzed with a line-confocal spectrometer (Figure S7). A grating resolution of 0.1 nm was used for high resolution measurement, and a resolution of 0.8 nm was used for wideband measurement. All measurements were conducted at 22 ± 2 °C and 40 ± 5% relative humidity under ambient air.

We observed lasing action from 5IPA3 perovskites in the n = 4 but not n < 4 phases (Figure 3a). The physical origin of the suppressed lasing for n < 4 is discussed in Supplementary Note S1, which indicates that lower-n phases possess larger exciton binding energies and higher Mott transition densities. In addition, stronger exciton−phonon coupling likely contributes to enhanced nonradiative recombination.[46] As the pump energy increased, narrowband, single-mode stimulated emission at 852 nm emerged on top of the broad spontaneous emission centered at 838 nm, with clamping occurring above the threshold pump energy of 1 mJ/cm^2 (Figure 3b). The laser input−output curve (Figure 3c) exhibited typical kink behavior, and fitting with a rate equation model yielded a spontaneous emission factor of 10^{-3}. The line width decreased from 57 nm in spontaneous emission as lasing occurred (Figure 3d). The narrowest line width, measured with high-resolution grating, was approximately 0.3 nm, corresponding to a lasing Q factor of 2850. Rapid material degradation occurred at a pump fluence of approximately 6 mJ/cm^2 (Figure S8).

The smallest lasing microcrystal was approximately 4 μm in its longest dimension. Finite-difference time-domain (FDTD) simulations suggest the presence of a high-Q dielectric resonance mode in the 4-μm-sized particle, with near-field profiles resembling whispering gallery modes in the square cavity, as shown in Figure 3e. The refractive index of 5IPA3 (n = 4) was estimated to be 2.3, based on the weighted average of the refractive indices of (MA)SnI_3 layers (index = 2.86)[47] and typical organic spacer layers (index = 1.5).[40] The resonant mode had a cold cavity Q factor of 200, although experimental Q factors may be lower due to surface roughness, shape imperfections, and other factors. The calculated mode volume was 2 μm^3, which could be slightly overestimated due to the inherent field divergence of leaky cavity eigenmodes. The required gain (k/Q, where k is wavevector) coefficient for room-temperature lasing is approximately 800 cm^{-1}. Wide-field imaging of particles above the lasing threshold revealed interference patterns with bright four-sided edges (Figure 3f), consistent with the expected whispering gallery (WG) mode in a square cavity (Figure 3g).

PLASMONIC LASING IN AIR AT ROOM TEMPERATURE

To investigate potential plasmonic Purcell enhancement,[48] we evaluated microcrystals placed on an ultrasmooth gold substrate (Figure S9). Figure 4a shows that 5IPA3 microcrystals on gold substrates exhibited lasing action from both n = 3 and n = 4 microcrystals, with a lasing threshold ranging from 0.75 to 1.2 mJ/cm^2 and a spontaneous emission factor of 10^{-2}. The narrowest observed line width was ∼0.35 nm, corresponding to a lasing Q-factor of 2440. The laser spectra, input−output intensities, line width narrowing, linear polarization state, and spatial emission patterns for representative devices are presented in Figure 4 and Figures S10, S11, and S12. FDTD simulation showed a hybrid plasmonic−photonic mode with a cold cavity Q-factor of 50 and a mode volume of 3 × 10^{-19} m^3, yielding a Purcell factor of 2 (Figure S10). The intrinsic gain required for room-temperature lasing, considering the Purcell enhancement, is ∼1690 cm^{-1}. Similar lasing behavior on metallic substrates has been previously observed in $CsPbBr_3$[48] and III−V compounds,[49] where air gaps arising from substrate roughness naturally form dielectric barriers. In our case, the organic spacer and surface asperities (Figure S9) likely play a similar role, providing dielectric shielding that suppresses quenching and enables optical gain on Au. Plasmon-exciton coupling was evidenced by the appearance of wiggling patterns and spatial inhomogeneity of Purcell

https://doi.org/10.1021/acsphotonics.5c02285
ACS Photonics 2026, 13, 2367−2374

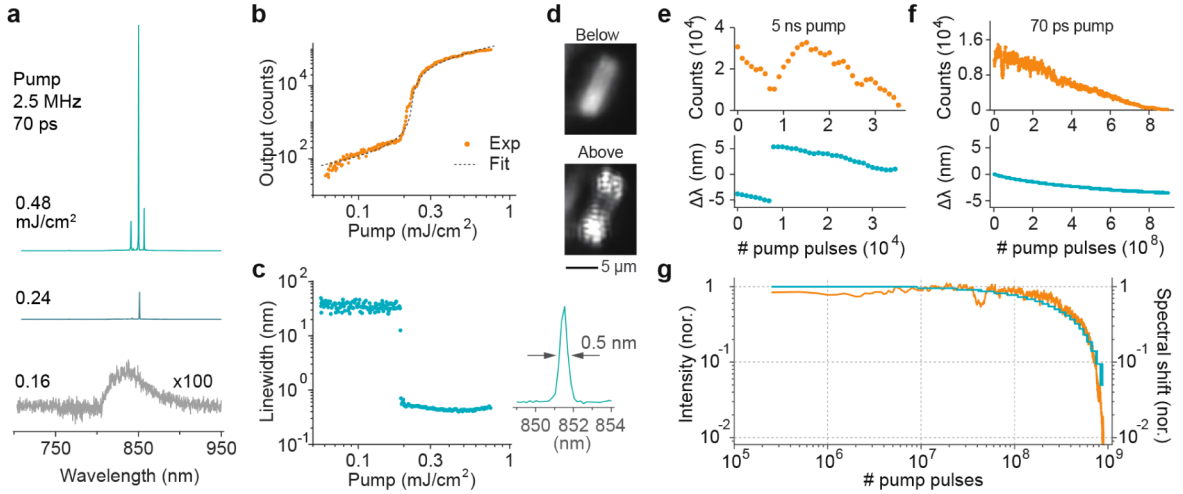

Figure 5. Laser stability in ambient conditions. (a) Output spectra of 5IPA3-n4 microcrystals on a gold substrate under picosecond pumping at various pump fluences: 0.16, 0.24, 0.36, and 0.48 mJ/cm^2. (b) Measured light-in-light-out curve. Dashed line: theoretical fit. (c) Measured line width at different pump fluences. (right) Emission spectra at 1.5 times the lasing threshold are shown. (d) Measured far-field emission profiles below and above the lasing threshold. (e) The intensity (top) and wavelength (bottom) variations of an n = 4 plasmonic device under nanosecond pumping. (f) Decay curves of another device under picosecond pumping at 1.5 times the lasing threshold. (g) Aging curves on a log scale for intensity (orange) and wavelength (green).

enhancement in the confocal fluorescence detection of n = 1 microcrystals near the plasmonic dispersion asymptote (Figure 4a and S13).[48]

Transient lifetime spectroscopy (120 ps resolution) revealed an accelerated lifetime in a double-exponential fit: 90.4% of 240 ps and 9.6% of 610 ps for microparticles on gold substrates compared to 86.5% of 410 ps and 13.5% of 1.4 ns for microparticles on thermal-oxide silicon substrates (Figure 4f). Assuming that the fastest channel corresponds to nonradiative decay and the slower one to radiative recombination, recombination on gold occurred approximately twice as fast, consistent with FDTD calculations. This Purcell enhancement increases the effective gain of the n = 3 devices, enabling even multimode lasing on plasmonic substrates, which is consistent with previous observations.[48,50]

PUMP EFFECT ON LASER STABILITY

We investigated picosecond pumping at 765 nm, near the band edge of n = 4 microcrystals on gold substrates, with a 2.5 MHz repetition rate (Figure 5a). The typical lasing threshold was 0.22 mJ/cm^2 per pulse, about four times lower than that for nanosecond pumping (Figure 5b). The spontaneous emission factor was approximately 0.001. The line width at 1.5 times the threshold was 0.59 nm (Figure 5c), and interference patterns were observed above the threshold (Figure 5d). The narrower line width under picosecond pumping is mainly due to the reduced heat accumulation.

Next, we compared the laser emission stability of 5IPA3-n4 perovskites on a gold substrate under nanosecond and picosecond pumping. In a sample under nanosecond pumping, mode hopping occurred after ~10^4 shots, followed by a blue shift of 3 nm and a 90% intensity drop after ~3 × 10^4 shots (Figure 5e). Other samples exhibited a 1.83 nm blue shift with a 95% intensity drop (Figure S14). In contrast, under picosecond pumping, laser emission persisted for a half billion pump pulses (Figure 5f and S14). Figure 5g shows decay curves on a log scale, showing rapid degradation after 10^8 pulses.

DISCUSSION

The incorporation of the 5IPA3-based hydrogen-bonding network significantly enhanced the photostability of the 2D and quasi-2D TIPs. This improved stability enabled the first demonstration of room-temperature lasing in air from the 5IPA-n3 and 5IPA-n4 microcrystals. Previously, lasing from n = 1 tin-iodide 2D perovskite nanowires with similar hydrogen-bonding organic sublattices[27] was achieved only at 88 K under an inert atmosphere. Room-temperature lasing was observed from n = 2 quasi-2D TIP exfoliated flakes in nitrogen, with a line width of ~2 nm and a threshold of around 0.4 mJ/cm^2.[26] All of these prior demonstrations relied on inert gas protection. Furthermore, these earlier systems required threshold peak power on the order of GW/cm^2, much higher compared to the kW to MW/cm^2 thresholds typical for 3D $CsPbBr_3$ and $MAPbI_3$ microlasers. In contrast, our 5IPA-based quasi-2D TIPs achieved lasing in air with a lower threshold of ~200 kW/cm^2 (Table S3 and Figure S15). We believe that the high quality of the microplates—characterized by excellent phase purity, precise morphology control through recently developed molecular templating methods,[27] and passivation with 5IPA3 organic spacers—substantially enhances their optical gain and stability. Although no encapsulation was used, the devices sustained lasing for over 10^8 pulses in ambient air. Encapsulation such as organic polymeric coating[51] or noble metal[52] coating could further enhance lifetime for device integration. This result highlights a major step toward practical device operation. In addition, we reported the first plasmonic lasing in TIPs. The optical gain coefficients of 5IPA3-n3 and 5IPA3-n4 TIPs are estimated to exceed 1000 cm^{-1}. We hypothesize that longer exciton diffusion lengths and enhanced intralayer energy transport in high-n TIPs contribute to a stronger Purcell effect near gold substrates for hybrid plasmonic−photonic modes. This work provides a foundation for future efforts in spacer engineering and material optimization toward practical photonic and optoelectronic applications.

https://doi.org/10.1021/acsphotonics.5c02285
ACS Photonics 2026, 13, 2367−2374

■ ASSOCIATED CONTENT

Supporting Information

The Supporting Information is available free of charge at https://pubs.acs.org/doi/10.1021/acsphotonics.5c02285.

Materials and methods; Precursor and solvent composition for layered perovskite microcrystal growth (Table S1); SEM analysis and size statistics of 5IPA3-n4 microcrystals (Figures S1−S2); Temperature-dependent photoluminescence and exciton binding energy extraction (Figure S3); Layer-number dependence of Mott carrier density (Note S1, Figure S4); Air-stability characterization of films and microcrystals (Figures S5−S6, Table S2); Laser optical characterization and damage threshold (Figures S7−S8); Plasmonic laser device characterization and simulations (Figures S9−S14); Comparison of 2D perovskite laser devices (Table S3, Figure S15) (PDF)

■ AUTHOR INFORMATION

Corresponding Authors

Letian Dou − *Davidson School of Chemical Engineering, Purdue University, West Lafayette, Indiana 47907, United States; Department of Chemistry, Purdue University, West Lafayette, Indiana 47907, United States; Department of Chemistry, Emory University, Atlanta, Georgia 30322, United States;* orcid.org/0000-0001-6411-8591; Email: letian.dou@emory.edu

Seok-Hyun Yun − *Wellman Center for Photomedicine, Massachusetts General Hospital, Cambridge, Massachusetts 02139, United States; Harvard Medical School, Boston, Massachusetts 02139, United States; Harvard-MIT Health Sciences and Technology, Cambridge, Massachusetts 02139, United States;* orcid.org/0000-0002-8176-9916; Email: syun@hms.harvard.edu

Authors

Sangyeon Cho − *Wellman Center for Photomedicine, Massachusetts General Hospital, Cambridge, Massachusetts 02139, United States; Harvard Medical School, Boston, Massachusetts 02139, United States;* orcid.org/0000-0002-2997-4760

Wenhao Shao − *Davidson School of Chemical Engineering, Purdue University, West Lafayette, Indiana 47907, United States; Department of Chemistry, University of Georgia, Athens, Georgia 30602, United States;* orcid.org/0000-0002-5237-0076

Jeong Hui Kim − *Davidson School of Chemical Engineering, Purdue University, West Lafayette, Indiana 47907, United States;* orcid.org/0009-0002-1206-5621

Complete contact information is available at: https://pubs.acs.org/10.1021/acsphotonics.5c02285

Author Contributions

[¶]S.C. and W.S. contributed equally to this work. S.C., W.S., L.D., and S.-H.Y. designed the study. W.S. and J.K. synthesized the materials. W.S. characterized material properties. S.C. conducted the lasing experiments and modeling. S.C., W.S., L.D., and S.H.Y. wrote the manuscript.

Funding

This research was supported in part by funding from the National Institutes of Health (R01EB033155, R01EB034687, and K25CA301033) and from the US Department of Energy, Office of Basic Energy Sciences, under award no. DE-SC0022082.

Notes

This work has been previously submitted to a pre-print server as Cho, S.; Shao, W.; Kim, J.H.; Dou, L.; Yun, S.H. Air-Stable Room-Temperature Quasi-2D Tin Iodide Perovskite Microlasers. 2025, arXiv:2507.08180. arXiv. https://arxiv.org/abs/2507.08180 (accessed July 10, 2025).

The authors declare no competing financial interest.

■ ABBREVIATIONS

TIPs, tin iodide perovskites; LHP, lead halide perovskites; 2D, two-dimensional; PEA, phenylethylammonium; 2T+, bithiophenylethylammonium; 3T+, (2-([2,2″:5′,2″-terthiophen]-5-yl)ethan-1-aminium; BrCA3, 2-(2-bromo-5-carboxyphenoxy)-ethan-1-aminium; 5IPA3, 2-(3,5-dicarboxyphenoxy)ethan-1-aminium; MA, methylammonium; FA, formamidinium; CW, continuous-wave; FDTD, finite-difference time-domain; WG, whispering-gallery

■ REFERENCES

(1) Jena, A. K.; Kulkarni, A.; Miyasaka, T. Halide Perovskite Photovoltaics: Background, Status, and Future Prospects. *Chem. Rev.* **2019**, *119* (5), 3036−3103.

(2) Fakharuddin, A.; Gangishetty, M. K.; Abdi-Jalebi, M.; Chin, S.-H.; Bin Mohd Yusoff, A. R.; Congreve, D. N.; Tress, W.; Deschler, F.; Vasilopoulou, M.; Bolink, H. J. Perovskite Light-Emitting Diodes. *Nat. Electron.* **2022**, *5* (4), 203−216.

(3) Moon, J.; Mehta, Y.; Gundogdu, K.; So, F.; Gu, Q. Metal-halide Perovskite Lasers: Cavity Formation and Emission Characteristics. *Adv. Mater.* **2024**, *36* (20), 2211284.

(4) Chen, C.; Cheng, S.; Cheng, L.; Wang, Z.; Liao, L. Toxicity, Leakage, and Recycling of Lead in Perovskite Photovoltaics. *Adv. Energy Mater.* **2023**, *13* (14), 2204144.

(5) Maranghi, S.; Parisi, M. L.; Basosi, R.; Sinicropi, A. The Critical Issue of Using Lead for Sustainable Massive Production of Perovskite Solar Cells: A Review of Relevant Literature. *Open Res. Eur.* **2021**, *1*, 44.

(6) Noel, N. K.; Stranks, S. D.; Abate, A.; Wehrenfennig, C.; Guarnera, S.; Haghighirad, A.-A.; Sadhanala, A.; Eperon, G. E.; Pathak, S. K.; Johnston, M. B.; et al. Lead-free organic−inorganic tin halide perovskites for photovoltaic applications. *Energy Environ. Sci.* **2014**, *7* (9), 3061−3068.

(7) Cao, J.; Yan, F. Recent Progress in Tin-Based Perovskite Solar Cells. *Energy Environ. Sci.* **2021**, *14* (3), 1286−1325.

(8) Chung, I.; Song, J.-H.; Im, J.; Androulakis, J.; Malliakas, C. D.; Li, H.; Freeman, A. J.; Kenney, J. T.; Kanatzidis, M. G. $CsSnI_3$: Semiconductor or Metal? High Electrical Conductivity and Strong near-Infrared Photoluminescence from a Single Material. High Hole Mobility and Phase-Transitions. *J. Am. Chem. Soc.* **2012**, *134* (20), 8579−8587.

(9) Lanzetta, L.; Webb, T.; Zibouche, N.; Liang, X.; Ding, D.; Min, G.; Westbrook, R. J. E.; Gaggio, B.; Macdonald, T. J.; Islam, M. S.; et al. Degradation Mechanism of Hybrid Tin-Based Perovskite Solar Cells and the Critical Role of Tin (IV) Iodide. *Nat. Commun.* **2021**, *12* (1), 2853.

(10) Yu, B.; Chen, Z.; Zhu, Y.; Wang, Y.; Han, B.; Chen, G.; Zhang, X.; Du, Z.; He, Z. Heterogeneous 2D/3D Tin-halides Perovskite Solar Cells with Certified Conversion Efficiency Breaking 14%. *Adv. Mater.* **2021**, *33* (36), 2102055.

(11) Sanchez-Diaz, J.; Sánchez, R. S.; Masi, S.; Krecmarová, M.; Alvarez, A. O.; Barea, E. M.; Rodriguez-Romero, J.; Chirvony, V. S.;

Sánchez-Royo, J. F.; Martinez-Pastor, J. P. Tin perovskite solar cells with >1,300 h of operational stability in N2 through a synergistic chemical engineering approach. *Joule* **2022**, *6* (4), 861−883.
(12) Xiao, L.; An, T.; Deng, C.; Xu, X.; Sun, H. On Biosafety of Sn-Containing Halide Perovskites. *Energy Environ. Sci.* **2023**, *16* (5), 2120−2132.
(13) Macdonald, T. J.; Lanzetta, L.; Liang, X.; Ding, D.; Haque, S. A. Engineering Stable Lead-free Tin Halide Perovskite Solar Cells: Lessons from Materials Chemistry. *Adv. Mater.* **2023**, *35* (25), 2206684.
(14) Konstantakou, M.; Stergiopoulos, T. A Critical Review on Tin Halide Perovskite Solar Cells. *J. Mater. Chem. A Mater.* **2017**, *5* (23), 11518−11549.
(15) Yang, W.; Igbari, F.; Lou, Y.; Wang, Z.; Liao, L. Tin Halide Perovskites: Progress and Challenges. *Adv. Energy Mater.* **2020**, *10* (13), 1902584.
(16) Pitaro, M.; Tekelenburg, E. K.; Shao, S.; Loi, M. A. Tin Halide Perovskites: From Fundamental Properties to Solar Cells. *Adv. Mater.* **2022**, *34* (1), 2105844.
(17) Wu, G.; Liang, R.; Ge, M.; Sun, G.; Zhang, Y.; Xing, G. Surface Passivation Using 2D Perovskites toward Efficient and Stable Perovskite Solar Cells. *Adv. Mater.* **2022**, *34* (8), 2105635.
(18) Baek, S.; Yang, S. J.; Yang, H.; Shao, W.; Yang, Y.; Dou, L. Exciton Dynamics in Layered Halide Perovskite Light-Emitting Diodes. *Adv. Mater.* **2025**, *37*, 2411998.
(19) Gong, Y.; Yue, S.; Liang, Y.; Du, W.; Bian, T.; Jiang, C.; Bao, X.; Zhang, S.; Long, M.; Zhou, G. Boosting Exciton Mobility Approaching Mott-Ioffe-Regel Limit in Ruddlesden−Popper Perovskites by Anchoring the Organic Cation. *Nat. Commun.* **2024**, *15* (1), 1893.
(20) Yan, L.; Ma, J.; Li, P.; Zang, S.; Han, L.; Zhang, Y.; Song, Y. Charge-carrier Transport in Quasi-2D Ruddlesden−Popper Perovskite Solar Cells. *Adv. Mater.* **2022**, *34* (7), 2106822.
(21) Biswas, S.; Zhao, R.; Alowa, F.; Zacharias, M.; Sharifzadeh, S.; Coker, D. F.; Seferos, D. S.; Scholes, G. D. Exciton polaron formation and hot-carrier relaxation in rigid Dion-Jacobson-type two-dimensional perovskites. *Nat. Mater.* **2024**, *23*, 937−943.
(22) Xiao, X.; Zhou, J.; Song, K.; Zhao, J.; Zhou, Y.; Rudd, P. N.; Han, Y.; Li, J.; Huang, J. Layer Number Dependent Ferroelasticity in 2D Ruddlesden−Popper Organic-Inorganic Hybrid Perovskites. *Nat. Commun.* **2021**, *12* (1), 1332.
(23) Zhang, S.; Jin, L.; Lu, Y.; Zhang, L.; Yang, J.; Zhao, Q.; Sun, D.; Thompson, J. J. P.; Yuan, B.; Ma, K. Moiré Superlattices in Twisted Two-Dimensional Halide Perovskites. *Nat. Mater.* **2024**, *23*, 1222−1229.
(24) Liu, C.; Yang, Y.; Chen, H.; Spanopoulos, I.; Bati, A. S. R.; Gilley, I. W.; Chen, J.; Maxwell, A.; Vishal, B.; Reynolds, R. P.; et al. Two-Dimensional Perovskitoids Enhance Stability in Perovskite Solar Cells. *Nature* **2024**, *633* (8029), 359−364.
(25) Alvarado-Leanos, A. L.; Cortecchia, D.; Saggau, C. N.; Martani, S.; Folpini, G.; Feltri, E.; Albaqami, M. D.; Ma, L.; Petrozza, A. Lasing in Two-Dimensional Tin Perovskites. *ACS Nano* **2022**, *16* (12), 20671−20679.
(26) Li, Y.; Zhou, H.; Xia, M.; Shen, H.; Wang, T.; Gao, H.; Sheng, X.; Han, Y.; Chen, Z.; Dou, L. Phase-Pure 2D Tin Halide Perovskite Thin Flakes for Stable Lasing. *Sci. Adv.* **2023**, *9* (32), No. eadh0517.
(27) Shao, W.; Kim, J. H.; Simon, J.; Nian, Z.; Baek, S.-D.; Lu, Y.; Fruhling, C. B.; Yang, H.; Wang, K.; Park, J. Y.; et al. Molecular Templating of Layered Halide Perovskite Nanowires. *Science* **2024**, *384* (6699), 1000−1006.
(28) Deng, Y.; Zhang, Q.; Shi, C.; Toyoda, R.; Qu, D.-H.; Tian, H.; Feringa, B. L. Acylhydrazine-Based Reticular Hydrogen Bonds Enable Robust, Tough, and Dynamic Supramolecular Materials. *Sci. Adv.* **2022**, *8* (4), No. eabk3286.
(29) Park, J. Y.; Song, R.; Liang, J.; Jin, L.; Wang, K.; Li, S.; Shi, E.; Gao, Y.; Zeller, M.; Teat, S. J.; et al. Thickness Control of Organic Semiconductor-Incorporated Perovskites. *Nat. Chem.* **2023**, *15* (12), 1745−1753.
(30) Liang, Y.; Shang, Q.; Wei, Q.; Zhao, L.; Liu, Z.; Shi, J.; Zhong, Y.; Chen, J.; Gao, Y.; Li, M.; et al. Lasing from Mechanically Exfoliated 2D Homologous Ruddlesden−Popper Perovskite Engineered by Inorganic Layer Thickness. *Adv. Mater.* **2019**, *31* (39), 1903030.
(31) Zhou, H.; Feng, Q.; Sun, C.; Li, Y.; Tao, W.; Tang, W.; Li, L.; Shi, E.; Nan, G.; Zhu, H. Robust Excitonic Light Emission in 2D Tin Halide Perovskites by Weak Excited State Polaronic Effect. *Nat. Commun.* **2024**, *15* (1), 8541.
(32) De, A.; Mora Perez, C.; Liang, A.; Wang, K.; Dou, L.; Prezhdo, O.; Huang, L. Tunneling-Driven Marcus-Inverted Triplet Energy Transfer in a Two-Dimensional Perovskite. *J. Am. Chem. Soc.* **2024**, *146* (6), 4260−4269.
(33) Lou, X.; Li, Y.; Lei, H.; Zhang, Y.; Zhou, H.; Shi, E.; Zhu, H. Robust and Efficient Out-of-Plane Exciton Transport in Two-Dimensional Perovskites via Ultrafast Förster Energy Transfer. *ACS Nano* **2024**, *18* (31), 20659−20666.
(34) Xing, G.; Wu, B.; Wu, X.; Li, M.; Du, B.; Wei, Q.; Guo, J.; Yeow, E. K. L.; Sum, T. C.; Huang, W. Transcending the Slow Bimolecular Recombination in Lead-Halide Perovskites for Electroluminescence. *Nat. Commun.* **2017**, *8* (1), 14558.
(35) Gong, X.; Voznyy, O.; Jain, A.; Liu, W.; Sabatini, R.; Piontkowski, Z.; Walters, G.; Bappi, G.; Nokhrin, S.; Bushuyev, O.; et al. Electron−phonon interaction in efficient perovskite blue emitters. *Nat. Mater.* **2018**, *17* (6), 550−556.
(36) Geiregat, P.; Maes, J.; Chen, K.; Drijvers, E.; De Roo, J.; Hodgkiss, J. M.; Hens, Z. Using Bulk-like Nanocrystals to Probeintrinsic Optical Gain Characteristics of Inorganic Lead Halide Perovskites. *ACS Nano* **2018**, *12* (10), 10178−10188.
(37) Saba, M.; Cadelano, M.; Marongiu, D.; Chen, F.; Sarritzu, V.; Sestu, N.; Figus, C.; Aresti, M.; Piras, R.; Lehmann, A. G.; et al. Correlated electron−hole plasma in organometal perovskites. *Nat. Commun.* **2014**, *5*, 5049.
(38) Schlaus, A. P.; Spencer, M. S.; Miyata, K.; Liu, F.; Wang, X.; Datta, I.; Lipson, M.; Pan, A.; Zhu, X.-Y. How Lasing Happens in $CsPbBr_3$ Perovskite Nanowires. *Nat. Commun.* **2019**, *10* (1), 265.
(39) Tanghe, I.; Samoli, M.; Wagner, I.; Cayan, S. A.; Khan, A. H.; Chen, K.; Hodgkiss, J.; Moreels, I.; Thourhout, D. V.; Hens, Z.; et al. Optical Gain and Lasing from Bulk Cadmium Sulfide Nanocrystals through Bandgap Renormalization. *Nat. Nanotechnol.* **2023**, *18* (12), 1423−1429.
(40) Blancon, J.-C.; Stier, A. V.; Tsai, H.; Nie, W.; Stoumpos, C. C.; Traore, B.; Pedesseau, L.; Kepenekian, M.; Katsutani, F.; Noe, G. T. Scaling Law for Excitons in 2D Perovskite Quantum Wells. *Nat. Commun.* **2018**, *9* (1), 2254.
(41) Leijtens, T.; Prasanna, R.; Gold-Parker, A.; Toney, M. F.; McGehee, M. D. Mechanism of Tin Oxidation and Stabilization by Lead Substitution in Tin Halide Perovskites. *ACS Energy Lett.* **2017**, *2* (9), 2159−2165.
(42) Liang, H.; Yuan, F.; Johnston, A.; Gao, C.; Choubisa, H.; Gao, Y.; Wang, Y.; Sagar, L. K.; Sun, B.; Li, P. High Color Purity Lead-free Perovskite Light-emitting Diodes via Sn Stabilization. *Adv. Sci.* **2020**, *7* (8), 1903213.
(43) Li, Y.; Li, Z.; Han, Y.; Lai, R.; Yao, J.; Li, C.; Xia, M.; Zhou, H.; Sheng, X.; Li, B.; et al. Dual Oxidation Suppression in Lead-Free Perovskites for Low-Threshold and Long-Lifespan Lasing. *Adv. Mater.* **2025**, *37*, 2418931.
(44) Huang, L.; Ge, Z.; Zhang, X.; Zhu, Y. Oxygen-Induced Defect-Healing and Photo-Brightening of Halide Perovskite Semiconductors: Science and Application. *J. Mater. Chem. A Mater.* **2021**, *9* (8), 4379−4414.
(45) Udalova, N. N.; Fateev, S. A.; Nemygina, E. M.; Zanetta, A.; Grancini, G.; Goodilin, E. A.; Tarasov, A. B. Nonmonotonic Photostability of $BA_2MA_{n-1}Pb_nI_{3n+1}$ Homologous Layered Perovskites. *ACS Appl. Mater. Interfaces* **2021**, *14* (1), 961−970.
(46) Luo, D.; Su, R.; Zhang, W.; Gong, Q.; Zhu, R. Minimizing Non-Radiative Recombination Losses in Perovskite Solar Cells. *Nat. Rev. Mater.* **2020**, *5* (1), 44−60.

https://doi.org/10.1021/acsphotonics.5c02285
ACS Photonics 2026, 13, 2367−2374

(47) Singh, J. K.; Mandal, S. K.; Banerjee, G. Refractive Index of Different Perovskite Materials. *J. Mater. Res.* **2021**, *36*, 1773−1793.
(48) Cho, S.; Yang, Y.; Soljačić, M.; Yun, S. H. Submicrometer Perovskite Plasmonic Lasers at Room Temperature. *Sci. Adv.* **2021**, *7* (35), No. eabf3362.
(49) Cho, S.; Martino, N.; Yun, S.-H. Half-Wave Nanolasers and Intracellular Plasmonic Lasing Particles. *Nat. Nanotechnol.* **2025**, *20* (3), 404−410.
(50) Yang, S.; Bao, W.; Liu, X.; Kim, J.; Zhao, R.; Ma, R.; Wang, Y.; Zhang, X. Subwavelength-Scale Lasing Perovskite with Ultrahigh Purcell Enhancement. *Matter* **2021**, *4* (12), 4042−4050.
(51) Cho, S.; Yun, S. H. Poly (Catecholamine) Coated $CsPbBr_3$ Perovskite Microlasers: Lasing in Water and Biofunctionalization. *Adv. Funct Mater.* **2021**, *31* (27), 2101902.
(52) Cho, S.; Yan, H.; Yun, S. H. Noble Metal Coating on Perovskite Microcrystals for Robust and Plasmonic Lasing Applications. *Adv. Opt Mater.* **2025**, *13*, 2403316.

https://doi.org/10.1021/acsphotonics.5c02285
ACS Photonics 2026, 13, 2367−2374